Monthly Notices
of the
ROYAL ASTRONOMICAL SOCIETY
MNRAS **441,** 671–680 (2014) doi:10.1093/mnras/stu610

Analysis of blueshifted emission peaks in Type II supernovae

J. P. Anderson,[1,2★] L. Dessart,[3] C. P. Gutierrez,[2,4] M. Hamuy,[2,4] N. I. Morrell,[5] M. Phillips,[5] G. Folatelli,[6] M. D. Stritzinger,[7] W. L. Freedman,[8] S. González-Gaitán,[2] P. McCarthy,[8] N. Suntzeff[9] and J. Thomas-Osip[5]

[1]*European Southern Observatory, Alonso de Cordova 3107, Vitacura, Santiago, Chile*
[2]*Departamento de Astronomía, Universidad de Chile, Casilla 36-D, Casilla 19001, Santiago, Chile*
[3]*Laboratoire Lagrange, UMR7293, Université Nice Sophia-Antipolis, CNRS, Observatoire de la Côte d'Azur, F-06300 Nice, France*
[4]*Millennium Institute of Astrophysics, Casilla 36-D, Santiago,Chile*
[5]*Carnegie Observatories, Las Campanas Observatory, Casilla 601, La Serena, Chile*
[6]*Institute for the Physics and Mathematics of the Universe (IPMU), University of Tokyo, 5-1-5 Kashiwanoha, Kashiwa, Chiba 277-8583, Japan*
[7]*Department of Physics and Astronomy, Aarhus University, Ny Munkegade 120, DK-8000 Aarhus C, Denmark*
[8]*Observatories of the Carnegie Institution for Science, Pasadena, CA 91101, USA*
[9]*George P. and Cynthia Woods Mitchell Institute for Fundamental Physics and Astronomy, Department of Physics and Astronomy, Texas A&M University, College Station, TX 77843, USA*

Accepted 2014 March 26. Received 2014 March 20; in original form 2014 January 31

ABSTRACT

In classical P-Cygni profiles, theory predicts emission to peak at zero rest velocity. However, supernova spectra exhibit emission that is generally blueshifted. While this characteristic has been reported in many SNe, it is rarely discussed in any detail. Here, we present an analysis of Hα emission peaks using a data set of 95 Type II supernovae, quantifying their strength and time evolution. Using a post-explosion time of 30 d, we observe a systematic blueshift of Hα emission, with a mean value of $-2000\,\mathrm{km\,s^{-1}}$. This offset is greatest at early times but vanishes as supernovae become nebular. Simulations of Dessart et al. match the observed behaviour, reproducing both its strength and evolution in time. Such blueshifts are a fundamental feature of supernova spectra as they are intimately tied to the density distribution of ejecta, which falls more rapidly than in stellar winds. This steeper density structure causes line emission/absorption to be much more confined; it also exacerbates the occultation of the receding part of the ejecta, biasing line emission to the blue for a distant observer. We conclude that blueshifted emission-peak offsets of several thousand km $\mathrm{s^{-1}}$ are a generic property of observations, confirmed by models, of photospheric-phase Type II supernovae.

Key words: supernovae: general.

1 INTRODUCTION

Type II supernovae (SNe II henceforth) are classified through the presence of hydrogen Balmer lines in their spectra (see Minkowski 1941 for initial spectral classification of SNe, and Filippenko 1997 for a review). Spectral line formation occurring in optically thick, rapidly expanding ejecta produce spectral features to appear with a P-Cygni profile morphology. An observed P-Cygni profile is characterized by an absorption feature which is blueshifted, and an emission feature found closer to zero rest velocity. The blueshifted absorption feature occurs due to material moving towards the observer which obscures continuum emission in the line of sight. As line opacity acts in addition to continuum opacity, the velocity at maximum absorption gives an estimate of the photospheric velocity. In classical P-Cygni theory (see e.g. Sobolev 1960; Castor 1970), the profile emission peaks at the rest wavelength of the corresponding line, i.e. at zero Doppler velocity in the rest frame. However, as first noted in the early-time spectra of SN 1987A (Menzies et al. 1987), observations reveal emission peaks that are often blueshifted, by as much as several thousand km $\mathrm{s^{-1}}$ (also note that such blueshifts were briefly mentioned in Chevalier 1976). To explain this property in SN 1987A, Chugai (1988) presented a modified version of the standard model for line formation which allowed for diffuse reflection of resonance radiation by the SN photosphere. This observation was further outlined by Elmhamdi et al. (2003) for the case of the well-observed Type II-Plateau (II-P) SN 1999em, while similar blueshifted features have been discussed for SN 1988A (Turatto et al. 1993), and SN 1990K (Cappellaro et al. 1995). More recently, this observation was reported for the sub-luminous II-P SN 2009md (Fraser et al. 2011).

★ E-mail: janderso@eso.org

© 2014 The Authors
Published by Oxford University Press on behalf of the Royal Astronomical Society

Downloaded from http://mnras.oxfordjournals.org/ at Universidad de Chile on October 14, 2014

While the above summary shows that blueshifted emission peaks have been observed and documented in the past, it still appears to be a relatively unexplored feature in the SN community, especially given the large number of individual SN II studies which have now been published. Indeed, there are many cases where such blueshifts are present, and seen to evolve in published spectral sequences; yet, little or no discussion is found in the respective papers (see e.g. Hamuy et al. 2001; Leonard et al. 2002a,b; Bose et al. 2013)[1].

From the modelling point of view, Dessart & Hillier (2005a) presented a study of the formation of P-Cygni line profiles in SNe II based on non-local thermodynamic equilibrium (LTE) steady-state radiative transfer models. In contrast to Chugai (1988), these authors concluded that the emission-peak blueshift is intimately related to the steep density fall-off of SN ejecta, causing strong occultation and optical-depth effects. Since the work of Dessart & Hillier, CMFGEN has been augmented to incorporate time dependence in the radiative-transfer equation and in the statistical-equilibrium equations, allowing a full time-dependent solution for the SN radiation based on more physical models of the progenitor star and its terminal explosion (Dessart & Hillier 2008, 2010; Hillier & Dessart 2012). As discussed below, the basic conclusions and predictions on P-Cygni profile formation made by Dessart & Hillier are confirmed by recent models of II SNe that include these upgrades (Dessart et al. 2013). The comparison between such models and observed SN spectral features nourishes the discussion presented in this paper.

We present a systematic analysis of the Hα emission-peak wavelengths for SN II, and discuss these observations in terms of theoretical understanding and modelling of spectral line formation. We do this to bring attention to the frequency of such observations, and to outline how they may be used to foster a better understanding of SN II progenitor and explosion physics.

The paper is organized as follows. In the next section, the data sample used for analysis is discussed, together with a brief overview of reduction and analysis processes. Then in Section 3, our results on the distributions and evolution of Hα P-Cygni emission-peak velocities are presented. In Section 4, we outline the theoretical framework for understanding such features, and use numerical simulations to explain their measurement and observation. The physical origin of these observations is discussed in Section 5, where we also connect this property to other SN characteristics. Finally, we present our conclusions in Section 6.

2 DATA AND ANALYSIS METHODS

The data sample was obtained through various SN follow-up campaigns. These are: (1) the Cerro Tololo SN programme (PIs: Phillips & Suntzeff 1986–2003); (2) the Calán/Tololo SN programme (PI: Hamuy 1989–1993); (3) the Optical and Infrared Supernova Survey (PI: Hamuy 1999–2000); (4) the Carnegie Type II Supernova Program (PI: Hamuy 2002–2003); and (5) the Carnegie Supernova Project (CSP; Hamuy et al. 2006, PIs: Phillips & Hamuy 2004–2009). An initial analysis of the *V*-band light-curve morphologies of this sample has recently been published in Anderson et al. (2014), and we refer the reader to that paper for in-depth description of SN light-curve parameter measurements. In addition, an initial analysis of the spectral diversity of SNe II, concentrating on Hα profiles, was recently published in Gutierrez et al. (2014). The data taken from the above follow-up programmes used in the current analysis amounts to 646 optical wavelength spectra of 95 SNe II. From the above surveys, we excluded events classified as IIn, IIb and SN 1987A-like. Furthermore, we only include in the current analysis SNe which have well-constrained explosion epochs (see below), and more than two spectral observations during the photospheric phase. We note that the follow-up surveys contributing to the current sample were magnitude limited.

Spectra were reduced and extracted in the standard way, and the reader is referred to Folatelli et al. (2013) for a detailed outline of the procedures employed (see also Hamuy et al. 2006). These are analogous to those applied to the CSP SN Ia sample. In summary, 2D spectra were bias subtracted and flat fielded before 1D extraction using the *apall* task in IRAF. 1D spectra were then wavelength calibrated through observations of arc lamps, and were finally flux calibrated using observations of spectrophotometric standard stars. The typical rms of individual wavelength solutions is less than 0.4 Å, hence this uncertainty brings negligible error into the velocity estimations. The data base of spectra was obtained with many different telescopes and instruments. Typically, the extracted 1D spectra have wavelength resolutions between 5 and 8 Å, corresponding to velocity resolutions of 230–370 km s^{-1}. The S/N ratio of spectra vary, depending on object brightness and distance from the observer. In the majority of cases, the S/N of the 1D spectra near to the Hα wavelength region of interest is more than 20.

To proceed with measuring the wavelength (and therefore velocity) shift of Hα emission peaks, we take host galaxy heliocentric recession velocities from NED,[2] and use these to place the observed spectra on to the rest wavelength of the SNe. In addition, many SNe II show the presence of narrow emission lines in their spectra due to H II regions at the SN site. When available, these give a more accurate Doppler velocity for the SN environment. Hence, we measure the wavelength of these regions as (a) a sanity check of host galaxy recession velocities, and (b) to use these in place of host galaxy recession velocities where measurements are possible (this distribution is further discussed below, and is presented in Fig. 2).

The emission-peak wavelength of the SN Hα profile (and the wavelength of the narrow host H II region) in each spectrum of the sequence for each object is measured. This is done by employing the *splot* routine in IRAF.[3] Within *splot* the '*k*' measurement is used to fit a single Gaussian to the emission part of the P-Cygni profile. The presence of narrow Hα from an underlying H II region can complicate the measurement of this peak. Therefore, in cases where strong Hα emission dominates over the Hα from the SN, we do not include measurements from those spectra. Where narrow Hα is present but weaker, then this is removed from the spectra by simply tracing a line across the base of its flux. Once the above has been taken into consideration, we fit the emission multiple times, changing the wavelength range used, until a fit is found to be satisfactory 'by-eye' (i.e. that the peak of the Gaussian coincides with the peak of the emission). Through this process, measurements are obtained using a wavelength window of around $\pm$ 50–100 Å, around the wavelength of the peak emission. Once a peak wavelength is measured, it is converted to an SN velocity using the inferred

[1] At the proof stage of this paper Faran et al. (2014) posted a paper on to the archive which discussed observations of blue shifts of Hα emission peaks in a sample of 23 SN IIP, together with their physical origin.

[2] http://ned.ipac.caltech.edu/

[3] IRAF is distributed by the National Optical Astronomy Observatory, which is operated by the Association of Universities for Research in Astronomy (AURA) under cooperative agreement with the National Science Foundation.

Downloaded from http://mnras.oxfordjournals.org/ at Universidad de Chile on October 14, 2014

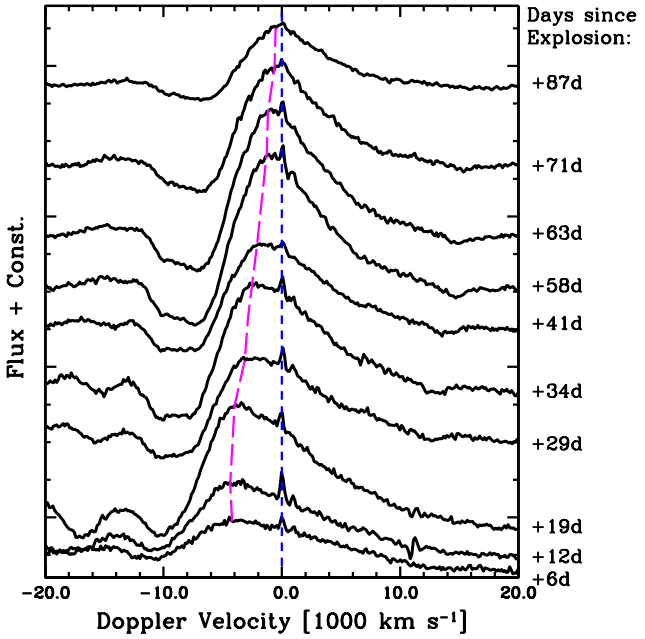

Figure 1. Hα spectral sequence of SN 2007X. The rest velocity of the SN position, as measured from the host H II region narrow Hα emission, is indicated by the short dashed blue line (i.e. at zero velocity). The long dashed magenta line shows the evolution of the Doppler velocity of the emission peak.

recession velocity, as described above. When the host galaxy recession velocity is employed, this brings a velocity error of ≈200 km s^{-1} (in extreme cases) due to the fact that recession velocities are measured at galaxy centres, while SNe explode at a range of galactocentric distances, and hence due to galaxy rotational velocities, could have rest velocities offset from those published in the literature (note, this is a very conservative error estimate; see Fig. 2). In addition, from our experience measuring peak emission wavelengths, any single spectral measurement has an error of several hundred km s^{-1} (due to the difficulty in defining the peak, together with the spectral resolution of each observation). Hence, we assume a conservative error of 500 km s^{-1} on all SN velocity measurements.

An example spectral sequence is shown in Fig. 1, where there is clear evidence for a significant blueshift of the SN Hα emission peak with respect to the narrow line from a coincident H II region. In addition, one observes a significant evolution of velocities with time, in particular of the emission-peak offset.

Before continuing to our results, we note that while this work concentrates on the observed wavelength/velocity of the Hα emission peak, significant velocity offsets are also found for the emission peaks of other spectral features. At early times, one observes very similar strength velocity offsets for the emission peak of Hβ. However, after several weeks post-explosion, an accurate measurement becomes impossible because of the increased effects of line blanketing, in particular the overlap with neighbouring Fe II lines. Hence, one cannot follow the evolution of Hβ emission velocity for more than a few weeks after explosion. Another complication is that some spectral features are absent at early times, and so only appear when line blanketing and line overlap are strong. This is for example a problem with the spectral feature at 4450 Å seen in the earliest spectra of SN 2006bp (Quimby et al. 2007) and SN 1999gi (Leonard et al. 2002b), which indeed models predict to be He II4686 Å but strongly blueshifted due to a very steep density gradient in the photospheric regions at early times (Dessart et al. 2008). Hα is by far the strongest line in emission in SN II spectra, and is present at all epochs. This line is thus ideally suited for the study presented here, and we continue using Hα as the tracer of velocity-shifted emission features for the remainder of this paper.

3 RESULTS

In Fig. 2 (top panel), the distribution of velocities of narrow Hα emission (associated with the coincident H II region) with respect to host galaxy recession velocities is presented. This distribution

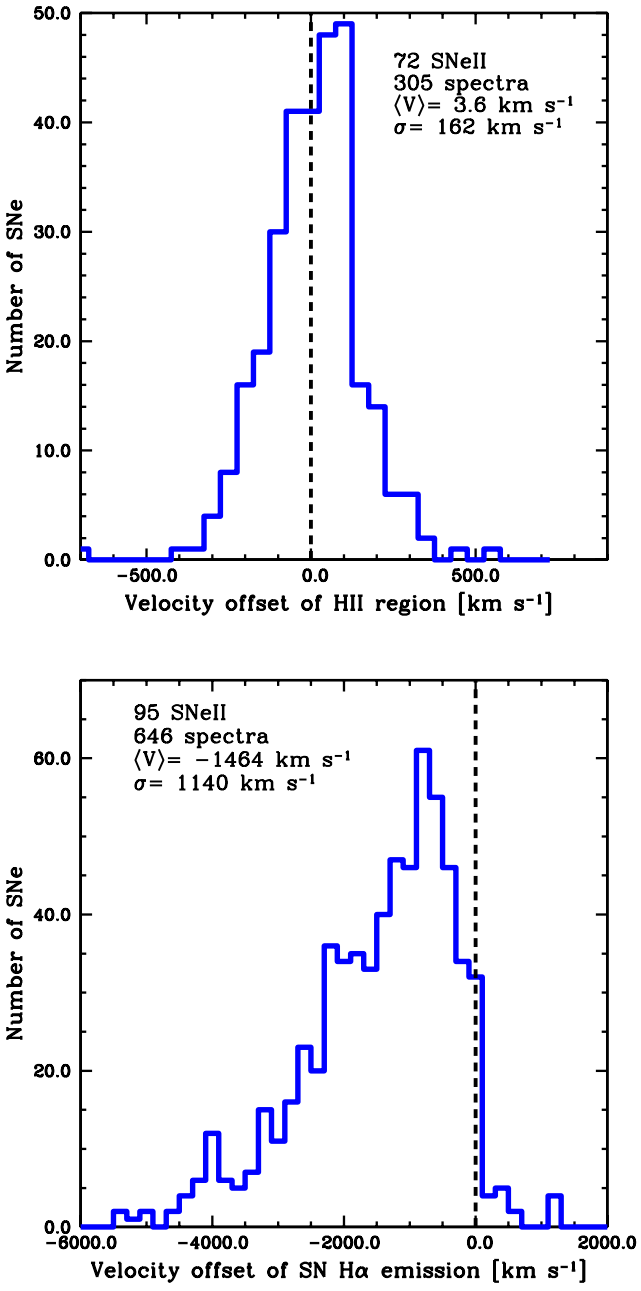

Figure 2. Top: histogram showing the velocity of the narrow peak emission (associated with a coincident H II region) detected in each SN spectrum, and given with respect to the host galaxy recession velocity. Bottom: histogram of the distribution of velocity offsets of Hα SN emission for the entire sample of SN II spectra (corresponding to different post-explosion epochs).

Downloaded from http://mnras.oxfordjournals.org/ at Universidad de Chile on October 14, 2014

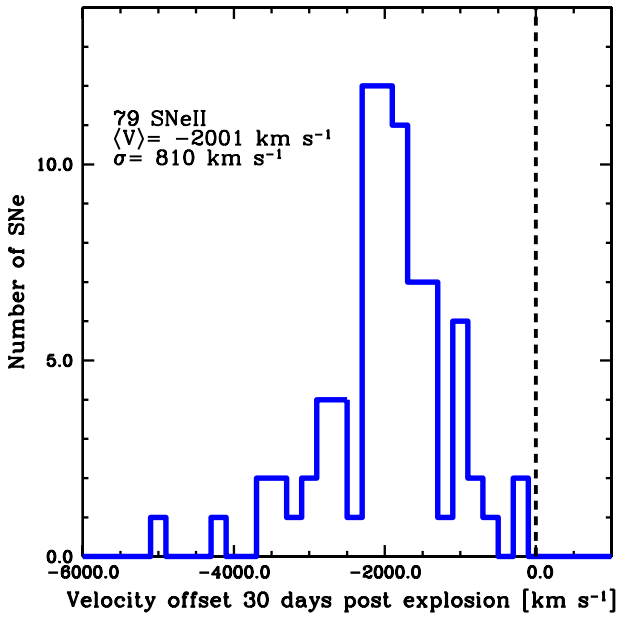

Figure 3. Histogram of the distribution of SN Hα emission velocity offsets for observations at 30 d after explosion.

contains 305 spectra for 72 SNe II in our sample, and the mean velocity offset is 4 km s^{-1}, i.e. essentially zero. The standard deviation of this distribution is 162 km s^{-1}. These values match expectations, since published host galaxy recession velocities will generally be velocities for the centre of each galaxy, whereas SNe will be distributed throughout the galaxy and hence will be found at velocities with a distribution centred on zero and a standard deviation equal to expected rotational velocities of spiral galaxies.

In Fig. 2 (bottom panel), we present the velocity offset distribution of the (broad) SN Hα emission peaks for *all* SNe spectra within our sample. It is immediately apparent that the distribution is heavily offset to significant negative velocities. Indeed, only 4 per cent of events have positive velocities (redshifted emission peaks). The mean velocity offset is −1464 km s^{-1} with a standard deviation of 1140 km s^{-1}.

As noted above, when one observes spectral sequences of SNe II, it is quite obvious that the blueshift of lines evolves significantly with time. In Fig. 1, this evolution is shown for SN 2007X. To compare SNe in terms of absolute blueshifted velocities, one needs to measure such a velocity at a consistent epoch. We adopt a post-explosion time of 30 d, where explosion epoch estimates are taken from Anderson et al. (2014), and interpolate measured velocities to this time. This early epoch is used because it corresponds to times when the diversity of blueshifted velocities is high (see Fig. 4). It also allows a significant fraction of the SN sample to be included, because numerous SNe in our sample lack spectroscopic data prior to a month after explosion. We note that the typical errors on our explosion epochs are ±6 d (taken from Anderson et al. 2014). The epochs used to interpolate velocities to 30 d are generally within ∼5–15 d either side of this epoch. The distribution of velocity offsets at 30 d post-explosion is presented in Fig. 3. The startling feature of this plot is that SNe have exclusive blueshifted velocities at this epoch. Indeed, the mean of the distribution is −2001 km s^{-1} with a standard deviation of 810 km s^{-1}. The other interesting feature of the figure is the high-velocity tail out to ∼4000 km s^{-1}. The overriding conclusion from the distributions presented above is that significant blueshifted emission velocities of the order of several thousand km s^{-1} are a ubiquitous feature in SN II spectra.

After presenting the distribution of the velocity offsets of Hα emission peaks at a representative post-explosion epoch, we now turn our attention to their evolution with time. In Fig. 4, this evolution is displayed for all 95 SNe in our sample. While there is significant scatter at all epochs, a number of interesting features are observed. First, the highest velocities are exclusively seen at early times. Very few SNe show blueshifted emission peaks higher than 2000 km s^{-1} after 50 d post-explosion, while at early times there is a significant number of SNe with velocities in excess of 3500 km s^{-1}. Secondly, the dispersion in velocity appears to decrease significantly with time.

In summary, significant blueshifted velocities of several thousand km s^{-1} are a very common feature of SN II spectra. These velocities evolve in time quite uniformly between SNe, eventually nearing zero as they progress to the end of the photospheric phase. In the following section, we discuss model spectra known to match the basic properties of SNe II-P (Dessart et al. 2013), as well as the theoretical framework for understanding the origin of emission-peak blueshifts.

4 INSIGHTS FROM RADIATIVE-TRANSFER SIMULATIONS

4.1 Previous studies with CMFGEN

As documented in the previous section, the offset of P-Cygni profile emission to the blue is a ubiquitous feature of all SNe II observed during the photospheric phase. In this section, we investigate whether this generic property is also present in spectra produced by radiative-transfer simulations of SNe II.

Spectrum formation for SNe II has been studied previously with CMFGEN. In Dessart & Hillier (2005a,b), steady-state non-LTE simulations were used to discuss the physics of P-Cygni profile formation in early-time spectra of SNe 1987A and 1999em. The peak blueshift is reproduced for both events prior to the recombination phase, and a detailed discussion of the origin of this property is given in section 5 of Dessart & Hillier (2005b). Later, in Dessart & Hillier (2008), the discussion is extended to more advanced photospheric-phase epochs, when the photospheric layers recombine, using a time-dependent solver for the non-LTE rate equations. This study focused primarily on the importance of time-dependent ionization, and in particular its role for producing a strong Hα line at the recombination epoch – little emphasis was put on the peak blueshift.

In Dessart et al. (2013), the radiative transfer in CMFGEN was improved by combining non-LTE and time dependence (for the non-LTE rate equations and the moments of the radiative-transfer equation). In addition, the computation is then performed on physically consistent (although piston driven) hydrodynamical explosions (see Hillier & Dessart 2012 for details and Dessart & Hillier 2010 for an application to SN 1987A). Moreover, these simulations cover a range of progenitor evolution and explosion properties for a 15 $M_{\odot}$ main-sequence star model and therefore allow one to inspect a number of dependences on SN II-P radiation properties.

In this paper, we inspect the simulations of Dessart et al. (2013), with a special focus on the evolution of line profile morphology from early photospheric epochs to the onset of the nebular phase. We focus on a representative sample of models, namely s15N, m15r1, m15r2, m15os, m15mlt1, m15mlt3, m15, m15e3p0, m15e0p6 and m15Mdot (see Dessart et al. 2013 for details; these models cover

Downloaded from http://mnras.oxfordjournals.org/ at Universidad de Chile on October 14, 2014

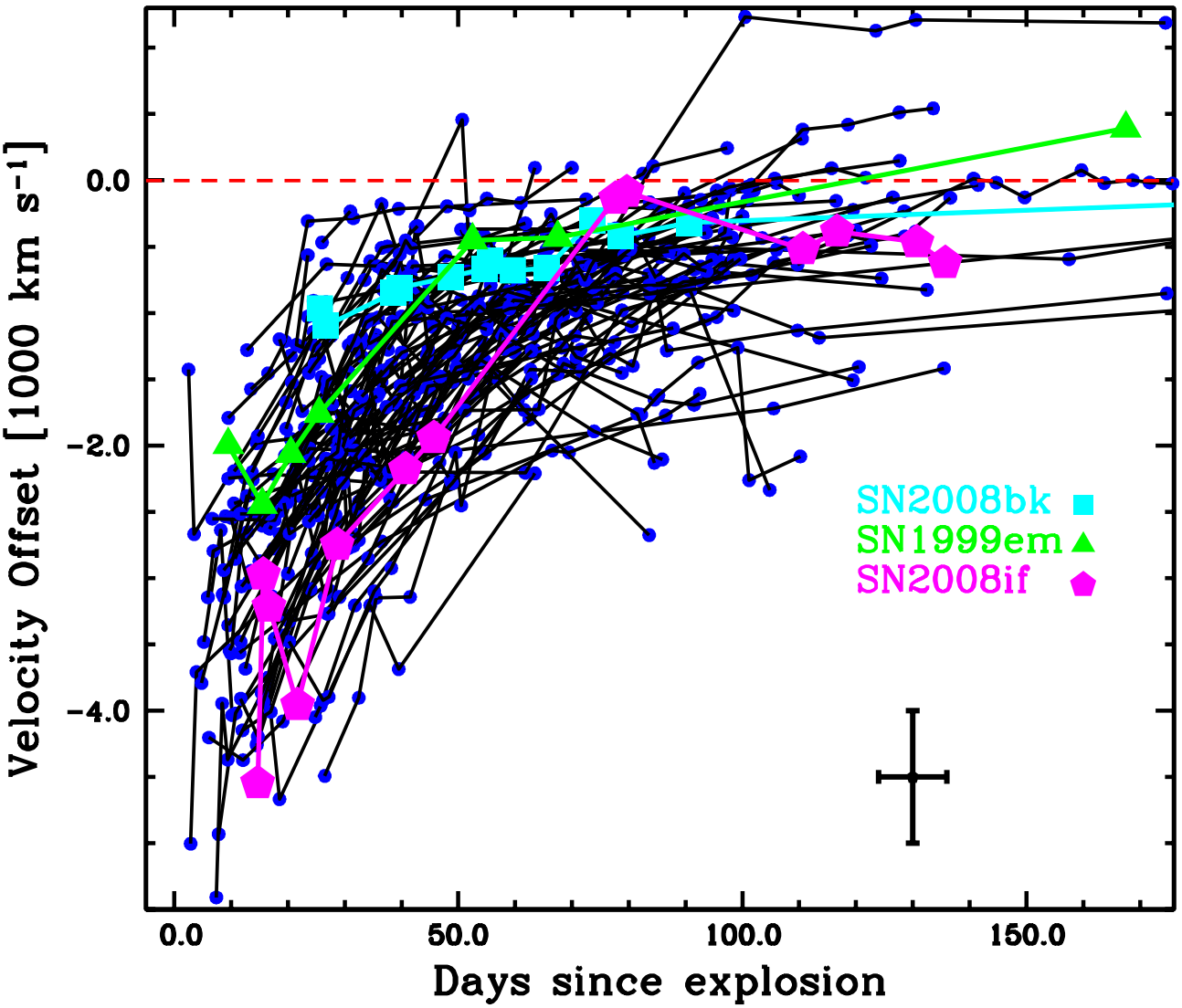

Figure 4. Evolution in time of the velocity offset of SN Hα emission peaks for the 95 SNe II in the current sample. Three events are shown: a sub-luminous event, SN 2008bk; a prototype Type II-P, SN 1999em; and a faster declining event, SN 2008if. A standard error bar for all measurements is given in black, where the origin of the velocity error is outlined in Section 2, and the time error is based on average errors of estimated explosion epochs (see Anderson et al. 2014 for a detailed description of that process).

a range of properties for the same main-sequence star mass but different initial rotation rate, mixing-length parameter, core overshooting prescription or explosion energy). We also include model m15mlt1x3, which is evolved the same way as m15 but with a mixing-length parameter of 1.5 and a mass-loss enhanced by a factor of 3 compared to the standard red supergiant (RSG) mass-loss rates provided by the 'DUTCH' recipe in MESA. This produces a low envelope-mass RSG at the time of explosion, which, when exploded to yield a 1.2 B ejecta kinetic energy, yields a II-Linear light-curve morphology (see Hillier et al., in preparation).

4.2 Results for SN II-P simulations

The first important result is that the peak-emission blueshift, observed in spectra of SNe II (see, e.g. Fig. 1) is also predicted by simulations at all times prior to the onset of the nebular phase. Fig. 5 shows the evolution of the Hα region from 11 d until 138 d after explosion in model m15mlt3. This model matches well the spectral and light-curve evolution of SN 1999em, except for a prolonged plateau phase of $\lesssim$150 d, which stems for the underestimated RSG mass loss in the MESA model (see Dessart et al. 2013 for details). The evolution of the velocity offset of peak emission agrees qualitatively and quantitatively with the observations. Importantly, all the simulations presented in Dessart et al. (2013) show the same behaviour, in agreement with observations (Fig. 6). Typical peak blueshifts are of the order of $-3200\,\mathrm{km\,s^{-1}}$ at 10 d after explosion and steadily decrease in strength to eventually reach zero at the end of the plateau, as observed.

5 DISCUSSION

In previous sections, it has been shown that significant blueshifted velocities of Hα emission peaks are a common feature of both observations *and* models of SNe II. Here, we first discuss the physical origin of these features and their diversity, before

Downloaded from http://mnras.oxfordjournals.org/ at Universidad de Chile on October 14, 2014

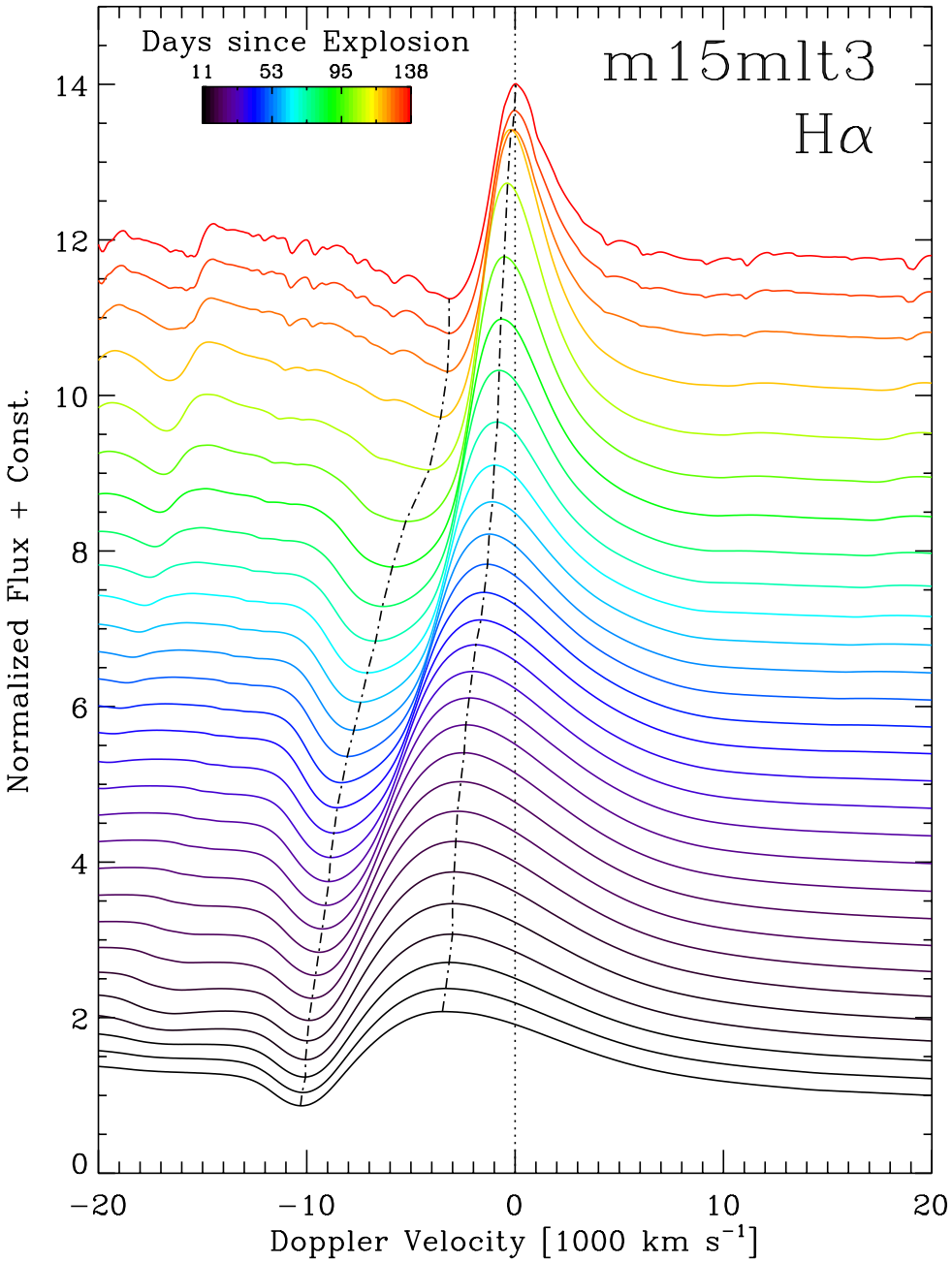

Figure 5. Evolution of the Hα spectral region from 11 d (bottom curve) until 138 d (top curve) after explosion in the SN II-P model m15mlt3 (Dessart et al. 2013). The abscissa is the Doppler velocity with respect to Hα. Individual times are colour coded, and the time difference between consecutive models is 10 per cent of the current time. The two broken lines track the location of maximum absorption and peak emission in Hα. The peak blueshift, strong at early times, decreases as the spectrum formation region recedes, and eventually becomes zero at the end of the plateau phase (in this model at ∼140 d).

presenting two correlations of this property with other SNe II transient measurements.

5.1 The physical origin of blueshifted emission peaks

In contrast to Chugai (1988), the origin of peak-emission blueshift seems to stem fundamentally from the steep density profile that characterizes SN ejecta layers, which were originally part of the H-rich envelope. In our simulations, this density distribution is well represented above ∼2000 km s^{-1} (which is roughly where the outer edge of the former He core lies in 1.2 B explosions of 15 M$_\odot$ RSG stars; Dessart, Livne & Waldman 2010) by a power law $\rho(v) \propto 1/v^n$, with exponent n of the order of 8. As a consequence, line emission tends to be confined in space, and subject to strong occultation effects for a distant observer. Instead of coming predominantly from the regions with large impact parameter p relative to the photospheric radius $R_{\rm phot}$, the bulk of the emission arises from rays with $p < R_{\rm phot}$, i.e. impacting the photodisc limited by $p = R_{\rm phot}$. As explained in Dessart & Hillier (2005a), the line source function tends to exceed the continuum source function at the continuum photosphere, naturally leading to line emission above the continuum flux level. Because electron scattering dominates the opacity, line

Downloaded from http://mnras.oxfordjournals.org/ at Universidad de Chile on October 14, 2014

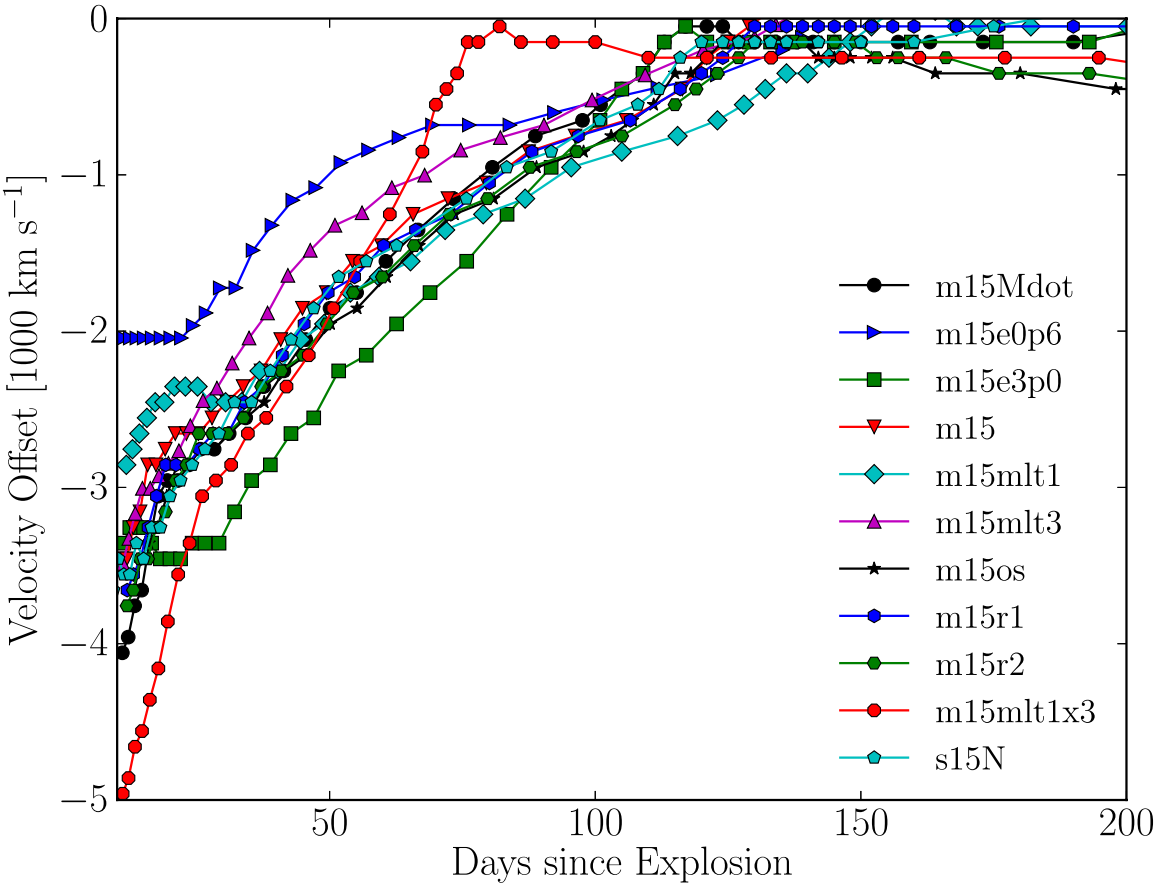

Figure 6. Evolution of the velocity offset of Hα peak emission with respect to rest wavelength for the large set of models presented in Dessart et al. (2013). All models follow the same trajectory, except for models m15e3p0/m15e0p6 (3 and 0.6 B, respectively), which have a larger/lower ejecta energy than other models (i.e. 1.2 B), and for model m15mlt1x3, in which the RSG mass-loss was artificially increased by a factor of 3. (See the text for discussion.)

photons have a relatively low destruction probability and we can therefore see line emission from layers deeper than the continuum photosphere.

Fig. 7 illustrates these effects for model m15mlt3 at 11 d (left-hand panel). As time progresses, the situation evolves significantly for several reasons. The spectrum formation recedes to deeper layers in the ejecta, where the density profile is flatter, favouring extended emission above the continuum photosphere. The velocities are also lower, so any velocity offset becomes less conspicuous. Moreover, time-dependent ionization exacerbates this effect by making the line optical depth more slowly varying with radius/velocity (Dessart & Hillier 2008), also favouring extended line emission. Interestingly, it is in part the increase in the extension of the spectrum formation region that favours the rise of polarization at the end of the plateau phase in SNe II-P (Dessart & Hillier 2011).

Departures from the mean trajectory of the peak location in velocity space of emission peaks are visible for three models in Fig. 6. First, the two models with a lower/higher kinetic energies (models m15e0p6 and m15e3p0) show smaller/larger offsets, simply reflecting the contrast in ejecta velocity (same envelope mass M, but different kinetic energy E). In these, the peak blueshifts at 10 d after explosion are -2000 and $-3500\,\mathrm{km\,s^{-1}}$, respectively. Secondly, model m15mlt1x3, which has a higher ejecta kinetic energy to ejecta mass (same E of 1.2 B as the models of Dessart et al. 2013, but much lower H-envelope mass), shows a markedly different trajectory for the peak-emission offset. Because the expansion rate is much larger, the offset is large initially, but the reduced envelope mass makes the transition to nebular phase earlier, and at such times the offset is always found to be zero in our models. Thus, the rate of change of this offset is much larger in model m15mlt1x3. This is an interesting property which is also seen in observations. Indeed, SNe with a higher s_2 parameter (i.e., V-band light curves with steeper decline rates) also have larger initial velocity offsets (see Fig. 8).

5.2 Correlation with other SN properties

While a full investigation into how observations of blueshifted emission are related to other SN properties is beyond the scope of this paper, in this section we outline a couple of interesting correlations that have been found, and suggest how these may be used to further understand the nature of SNe II. In Fig. 8, the decline rate during the 'plateau', s_2 (which is a proxy for the degree to which an SN II could be classified as 'Linear'; see Anderson et al. 2014), is plotted against the SN emission-peak velocity offset measured at 30 d post-explosion (only SNe which have both s_1 – the initial decline from maximum – and s_2 defined are included, see Anderson et al. 2014 for justification of this). A correlation is found in that faster declining SNe show higher velocity offsets at the same epoch as compared to smaller s_2 SNe. To test the significance of this correlation, we employ a Monte Carlo application of the Pearson test for correlations (following the procedure outline in Anderson

Downloaded from http://mnras.oxfordjournals.org/ at Universidad de Chile on October 14, 2014

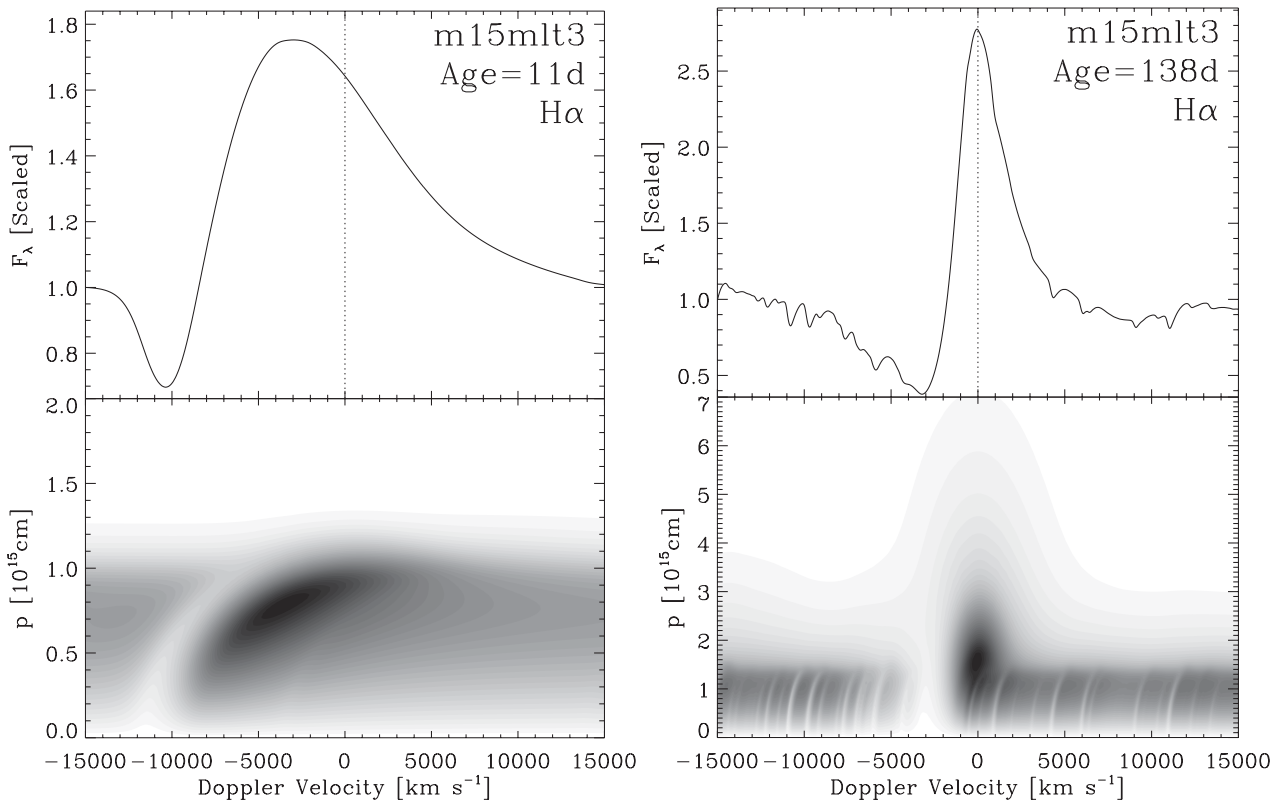

Figure 7. Distribution of the quantity $p \times I(p)$, as seen by a distant observer at rest, versus Doppler velocity v and impact parameter p (lower panels). When integrated over p, this gives the flux at v (upper panels). Here, we show an SN II-P model at 11 d (left) and 138 d (right) after explosion. The grey-scale maps thus reveal the origin of the emergent radiation in different profile regions (Doppler velocity) along rays with different p. The main reason for the blueshift is the confinement of emission within the column of material falling on to the 'photodisc'. This disc is limited on the plane of the sky by an impact parameter p of the order of $R_{\rm phot}$. Because of obscuration effects, and the lack of line emission at large impact parameters, the emission comes primarily from regions that are blueshifted, and this naturally leads to peak-emission blueshift. At late times (right-hand panel), obscuration effects are still present, but there is now significant emission at large impact parameters, which occurs symmetrically from approaching and receding regions. In fact, photon emission is more extended at all wavelengths, stemming both the former He core and the H-rich envelope.

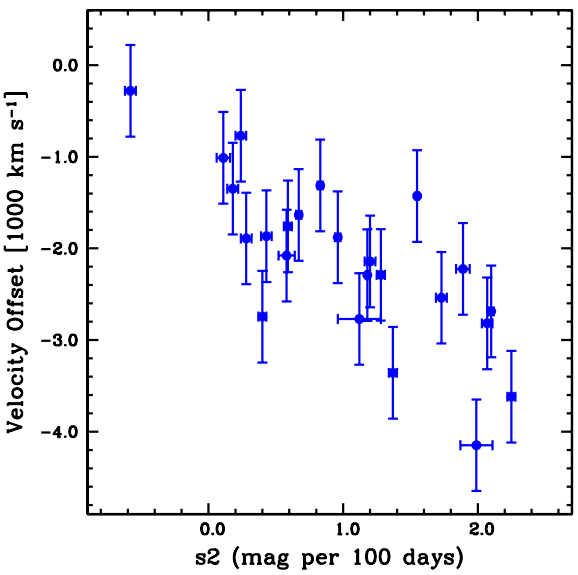

Figure 8. s_2 (the decline rate during the 'plateau') plotted against the velocity offset of SNe Hα emission peaks at 30 d post-explosion.

et al. 2014). A Pearson's r-value of -0.75 ± 0.10 is calculated, which, for $N = 24$ equates to a lower limit significance $P = 6 \times 10^{-4}$ (i.e. the probability of finding a correlation by chance). It is interesting that in the synthetic measurements displayed in Fig. 6, the highest velocity offsets at around 30 d post-explosion are for the model (m15mlt1x3), which has a more 'Linear' light-curve morphology (i.e. a high s_2). As discussed in Section 4.2, model m15mlt1x3 is characterized by the same ejecta kinetic energy of 1.2 B as other models from Dessart et al. (2013), but its ejecta mass is smaller. This translates to a higher expansion rate and a shorter photospheric phase duration, hence a larger Hα peak offset early on together with its more rapid decrease to zero.

In Fig. 9, SNe maximum V-band magnitudes are correlated against SN emission-peak velocity offsets measured at 30 d post-explosion. A strong correlation is found in terms of brighter SNe showing higher velocity offsets (confirmed by a Monte Carlo application of the Pearson test: $N = 51$, $r = 0.75 \pm 0.07$ $P < 2 \times 10^{-8}$). The strength of this correlation is quite remarkable, given the uncertainties in measurements of $M_{\rm max}$ (problems in defining this epoch, issues with host galaxy extinction corrections), the explosion epoch estimations (see discussion in Anderson et al. 2014), together with those of the velocity offsets. Here again, our more 'Linear' SN II model m15mlt1x3 offers a promising explanation (together

Downloaded from http://mnras.oxfordjournals.org/ at Universidad de Chile on October 14, 2014

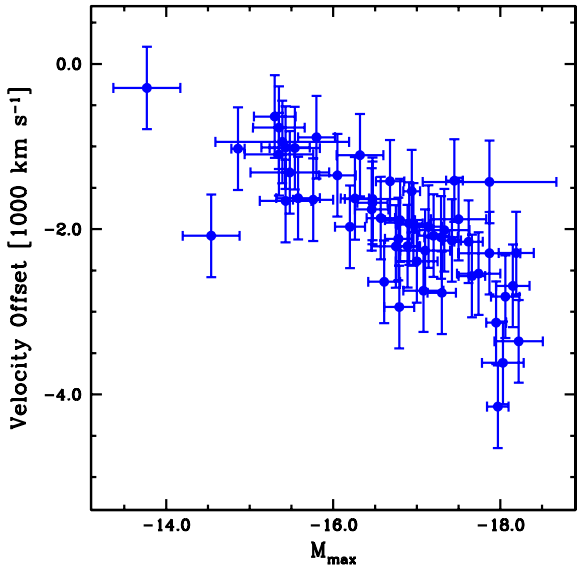

Figure 9. M_{max} (absolute magnitude at maximum light in the V band) plotted against the velocity offset of SNe Hα emission peaks at 30 d post-explosion.

with the possibility of diversity being related to explosion energy differences). Indeed, it exhibits a much higher luminosity than other SNe II-P models in Dessart et al. (2013), although it has the same explosion energy. The difference here is that this energy is coupled to a smaller progenitor envelope mass, leading to a higher energy per unit mass, a higher luminosity early on with a larger expansion rate. Because the ejecta mass is lower, the photospheric phase is shorter and so the luminosity decreases earlier and faster until reaching the nebular phase. In that context, this observation would support the notion that the diversity of SNe II-P, in particular the smooth connection to SNe II with more 'Linear' light curves (Anderson et al. 2014, although see Arcavi et al. 2012 for claims of a distinct separation between SNe II-P and SNe II-L), stems from a diversity in progenitor envelope mass. This hypothesis is discussed at length in Anderson et al. (2014) with respect to the diversity seen in the V-band light curves of 116 SNe II. Of course, this does not preclude the additional diversity stemming from varying explosion energies.

In the context of the current analysis, the diversity of the observed (and predicted) strength of blueshifted emission velocities can then be understood in terms of changes in the pre-SN envelope mass and/or differences in explosion energy. As one decreases the envelope mass (or increases the explosion energy), ejecta velocities increase due to the higher energy per unit mass. The strength of the blueshifted emission velocity is then directly linked to the ejecta velocity. This energy increase also increases the early luminosity (hence a higher M_{max}, as observed in Fig. 9), while the faster expansion leads to faster declining light curves, and hence the correlation observed with s_2 in Fig. 8.

Finally, we note that the correlation presented in Fig. 9 implies that measurements of the blueshift of Hα emission profiles could be used to predict SN absolute magnitudes. In this sense, such a correlation could be used as another SN II distance indicator method (to complement other such methods; e.g. Hamuy & Pinto 2002). The rms scatter of the trend found in Fig. 9 is ∼0.68 mag; however, one may hope to further improve this with a more detailed analysis (e.g. better constraints on host extinction, the use of colour information). As noted in Section 2, the follow-up surveys which contributed to the current sample were magnitude limited in nature. Hence, if the correlation presented in Fig. 9 holds, then surveys such as the CSP will preferentially follow SNe with larger blueshifted velocity offsets.

6 CONCLUSIONS

We have presented an observational analysis which shows that blueshifted emission peaks are seen in *all* spectral sequences of SNe II. These blueshifted velocity offsets are observed to be larger at early times and evolve to being consistent with zero, once SNe enter their nebular phase. Hence, peak-emission blueshifts are generic properties of observed SN II spectra. In addition, we demonstrate that emission-peak blueshifts are also a generic feature of photospheric-phase SN II spectra computed with the non-LTE time-dependent radiative-transfer code CMFGEN and based on physical models of the progenitor star and explosion. In fact, such blueshifts occur not just in SNe II, but also in SNe Ia (Blondin et al. 2006), although line overlap complicates a clear identification of such offsets. In SNe II, the velocity offset is best seen in Hα, because the line is strong, but also because one can track the velocity offset from being large early on to becoming negligible when the SN turns nebular.

In addition, we have shown that the diversity of blueshifted velocities found within a large sample of SNe II, can also be linked to SN II light-curve diversity. SNe showing larger blueshifts are also found to be brighter objects, and have faster declining light curves. We speculate that this diversity and the trends observed between different parameters, can be most easily understood in terms of differences in progenitor envelope masses retained before the epoch of explosion.

Until now, measurements, analysis and discussion of these properties for SNe of any kind have been scarce, despite the fact that their presence is obvious and systematic. As our analysis and discussion shows, these features and their evolution systematically change between SNe, and offer additional leverage to identify the origin of the diversity in SN II observations, progenitors, and explosion.

ACKNOWLEDGEMENTS

We thank the anonymous referee for his/her useful suggestions. This paper is based on observations obtained at the Gemini Observatory, which is operated by the Association of Universities for Research in Astronomy, Inc., under a cooperative agreement with the NSF on behalf of the Gemini partnership: the National Science Foundation (United States), the National Research Council (Canada), CONICYT (Chile), the Australian Research Council (Australia), Ministério da Ciência, Tecnologia e Inovação (Brazil) and Ministerio de Ciencia, Tecnología e Innovación Productiva (Argentina; Gemini Program GS-2008B-Q-56). This paper includes data gathered with the 6.5 metre Magellan Telescopes located at Las Campanas Observatory, Chile. Based on observations made with ESO telescopes at the La Silla Paranal Observatory under programmes: 076.A-0156, 078.D-0048, 080.A-0516 and 082.A-0526. JPA acknowledges support by CONICYT through FONDECYT grant 3110142, and by the Millennium Center for Supernova Science (P10-064-F), with input from 'Fondo de Innovación para la Competitividad, del Ministerio de Economía, Fomento y Turismo de Chile'. LD acknowledges financial support from the European Community through an International Re-integration Grant, under grant number PIRG04-GA-2008-239184, and from 'Agence Nationale de la Recherche' grant ANR-2011-Blanc-SIMI-5-6-007-01. The work

Downloaded from http://mnras.oxfordjournals.org/ at Universidad de Chile on October 14, 2014

of the CSP has been supported by the National Science Foundation under grants AST0306969, AST0607438 and AST1008343. MH and CG acknowledge support by projects IC120009 'Millennium Institute of Astrophysics (MAS)' and 'P10-064-F 'Millennium Center for Supernova Science' of the Iniciativa Científica Milenio del Ministerio Economía, Fomento y Turismo de Chile. MDS gratefully acknowledges generous support provided by the Danish Agency for Science and Technology and Innovation realized through a Sapere Aude Level 2 grant. This research has made use of the NASA/IPAC Extragalactic Database (NED) which is operated by the Jet Propulsion Laboratory, California Institute of Technology, under contract with the National Aeronautics.

REFERENCES

Anderson J. P. et al., 2014, preprint (arXiv:1403.7091)
Arcavi I. et al., 2012, ApJ, 756, L30
Blondin S. et al., 2006, AJ, 131, 1648
Bose S. et al., 2013, MNRAS, 433, 1871
Cappellaro E., Danziger I. J., della Valle M., Gouiffes C., Turatto M., 1995, A&A, 293, 723
Castor J. I., 1970, MNRAS, 149, 111
Chevalier R. A., 1976, ApJ, 207, 872
Chugai N. N., 1988, Sov. Astron. Lett., 14, 334
Dessart L., Hillier D. J., 2005a, A&A, 437, 667
Dessart L., Hillier D. J., 2005b, A&A, 439, 671
Dessart L., Hillier D. J., 2008, MNRAS, 383, 57
Dessart L., Hillier D. J., 2010, MNRAS, 405, 2141
Dessart L., Hillier D. J., 2011, MNRAS, 415, 3497
Dessart L. et al., 2008, ApJ, 675, 644
Dessart L., Livne E., Waldman R., 2010, MNRAS, 408, 827
Dessart L., Hillier D. J., Waldman R., Livne E., 2013, MNRAS, 433, 1745
Elmhamdi A. et al., 2003, MNRAS, 338, 939
Faran T. et al., 2014, preprint (arXiv:1404.0378)
Filippenko A. V., 1997, ARA&A, 35, 309
Folatelli G. et al., 2013, ApJ, 773, 53
Fraser M. et al., 2011, MNRAS, 417, 1417
Gutiérrez C. P. et al., 2014, preprint (arXiv:1403.7089)
Hamuy M., Pinto P. A., 2002, ApJ, 566, L63
Hamuy M. et al., 2001, ApJ, 558, 615
Hamuy M. et al., 2006, PASP, 118, 2
Hillier D. J., Dessart L., 2012, MNRAS, 424, 252
Leonard D. C. et al., 2002a, PASP, 114, 35
Leonard D. C. et al., 2002b, AJ, 124, 2490
Menzies J. W. et al., 1987, MNRAS, 227, 39P
Minkowski R., 1941, PASP, 53, 224
Quimby R. M., Wheeler J. C., Höflich P., Akerlof C. W., Brown P. J., Rykoff E. S., 2007, ApJ, 666, 1093
Sobolev V. V., 1960, Moving Envelopes of Stars. Harvard Univ. Press, Cambridge
Turatto M., Cappellaro E., Benetti S., Danziger I. J., 1993, MNRAS, 265, 471

This paper has been typeset from a TEX/LATEX file prepared by the author.

Downloaded from http://mnras.oxfordjournals.org/ at Universidad de Chile on October 14, 2014